On the morphogenesis of stellar flows

Application to planetary nebulae

D. Da Rocha[1] and L. Nottale[1]

[1]UMR CNRS 8631, LUTH, Observatoire de Paris-Meudon, F-92195 Meudon Cedex, France

Abstract

A large class of stellar systems (e.g., planetary nebulae (PNe), supernova envelopes, LBV stars, young stars in formation) shows structures in their accretion/ejection phase that have similar characteristics. In particular, one currently observes for these objects equatorial discs, axial ejections and stable bipolar shells. However these simple shapes, which are expected to be solutions of standard hydrodynamical equations, are not yet fully understood. In this paper, we suggest a new form of these equations that takes into account the fractality and the irreversibility of particle motion in such processes. Then we study in this framework a general infall or ejection motion in a central spherical potential. From the stationary solutions allowed by this new hydrodynamical system, we deduce a specific distribution of matter density, described in terms of probability density for ejection angles. A global classification of predicted shapes, depending on the values of conservative quantities such as (E^2, L^2, L_z), is given. These results are compared with the available observational data, and allows us to theoretically predict the possible existence of more complicated structures and of correlations between observable variables, which could be checked by future observations.

keywords: relativity - gravitation - hydrodynamic - planetary nebulae - LBV star - supernovae - star formation

1   Introduction

With the recent evolution of observational techniques, a great diversity of unexpected gravitational structures has spring up in many astrophysical domains. The large number and the stability of these structures has pointed out the incompleteness of their understanding in terms of standard approaches. This still represents a large and fundamental open problem. Moreover, one observes similar structures in many different systems, at many different scales and in various conditions characterizing the underlying medium, such as stable discs, rings, disc/jets combinations and bipolar outflows.

The present works on the formation and the dynamics of planetary nebulae are based on hydrodynamical collisions between slow and fast winds emitted at different stellar evolution stages. This is the Interacting Stellar Wind (ISW) model, generalized by Balick [2]. In this model, slow winds (10-20 km/s) are firstly emitted during the AGB phase then, at the end of this period, UV-radiations ionize this circumstellar slow medium. After this initial ejection, the stellar surface still losses its matter, but fast winds ($\approx$ 1000 km/s) are observed and enter in collision with slow winds. This collision induces a compressed zone where a hot bubble creates the observable bright shells of planetary nebulae. The spherical and elliptic shapes are satisfactorily understood in the framework of this description ([9], [16]), but the majority of the planetary nebula shapes cannot result from this model [13]. Despite the improvement of hydrodynamic simulations, even the simplest bipolar shells are not found to be formed in an universal way [3], since each particular case needs an ad-hoc hypothesis on the density of presumed slow equatorial winds and observed fast winds. Moreover, bright bipolar shells are not directly connected to the hot bubble resulting from the collision [2]. Thus, in the standard hydrodynamical approach, the initial hypothesis made about the nature of the slow and fast winds (which are connected to each central system studied) play a central role.

In the present paper, we shall explore a different though complementary approach to these problems. Independently of the initial wind densities, we can study the consequences of the specificity of individual trajectories of particles making the shells. We use a fluid-like description, in which the possible trajectories are non-deterministic. Because of the information loss due to collisions and to the continual ionization/diffusion of central star photons, individual particle trajectories can no longer be strictly followed, so that a statistical

description in terms of fractal and non-differentiable trajectories is adopted. Such a description finally gives a new form to the hydrodynamical equations.

2   Theory

In the following theoretical development, we use general hydrodynamical concepts, then we apply them to the specific case of an ejection process. It can be already noted that these solutions can be also used, with a mere time reversal, for describing infall motion in a spherical potential.

In a typical process of stellar mass ejection (developed above), the interaction between winds or ISM and the continual interaction of emitted photons allow one to set the following simple hypotheses:

(i) For each particle, the information about its trajectory is lost beyond some small space-scale and time-scale (compared with the global space-scale and time-scale of structuration of the system). Such a memory loss of the previous dynamical conditions is compatible with a fractal description using a fractal dimension $D_F = 2$ for trajectories (as in standard Brownian motion). Only global informations are conserved.

(ii) The test particles can follow an infinity of potential trajectories, and the study of such systems therefore comes under a fluid approach (like in their standard description).

(iii) The last main point is the irreversibility of this process. This irreversibility is local and global: for small scales, this is connected with the non-deterministic trajectories, and at the scale of the global system, this represents the impossibility for the system to come back to its initial conditions.

These three points can be summed up in terms of three fundamental conditions which lead to the construction of new hydrodynamic tools:

(i) The fractality of each individual trajectory beyond some transition scale. It is described in terms of elementary displacements which read:

$$dX = dx + d\xi, \qquad (1)$$

where $dx = vdt$ is a classical, differentiable variable, while $d\xi$ is a non-differentiable, stochastic variable, that describes the fractal fluctuation. Its non-deterministic character implies that it is known only through a statistical description. Namely, in the simplest case only considered here (fractal dimension 2), it is such that

$$< d\xi > = 0, \quad \text{and} \quad < d\xi^2 > = 2\mathcal{D}dt. \qquad (2)$$

Its non-differentiability is apparent here since $< d\xi^2 >^{1/2} /dt \propto dt^{-1/2}$ and it is therefore formally infinite. However, as we shall see, the fact that it vanishes

in the mean allows one to give a description in terms of only the differentiable part dx of the elementary displacement, that includes the indirect effects involved by the existence of the non-differentiable part. The coefficient $\mathcal{D}$ is a measure of the amplitude of the fractal fluctuations.

(ii) The test-particles can follow an infinity of possible trajectories: this leads one to jump to a non-deterministic, fluid-like description, in terms of the "classical part" of the velocity field of the family of trajectories, $v = v(x(t), t)$.

(iii) The reflection invariance under the transformation $(dt \leftrightarrow -dt)$ is broken as a consequence of the non-differentiability. Indeed, there are two definitions of velocity which are based on the variation of the position variable X either in the interval $[t - dt, t]$, or in the interval $[t, t + dt]$. The two definitions are equivalent in the differentiable case, but no longer in the non-differentiable one considered here. This leads to a two-valuedness of the velocity vector, (v_-, v_+). The use of a complex velocity, $\mathcal{V} = (v_+ + v_-)/2 - i(v_+ - v_-)/2$ to deal with this two-valuedness can be shown to be a covariant and simplifying representation (Nottale [20], Célérier [6]).

These three effects can be combined to construct a complex time derivative operator ([20], [21], [22]), that reads,

$$\frac{d'}{dt} = \frac{\partial}{\partial t} + \mathcal{V}.\nabla - i\mathcal{D}\triangle \qquad (3)$$

Now, we can use this new relation and follow the standard classical mechanics construction. A general Lagrange function $L(x, \mathcal{V}, t)$ characterizes any system and we define a general action $\mathcal{S}$ thanks to

$$\mathcal{S} = \int_{t_1}^{t_2} L(x, \mathcal{V}, t)\, dt. \qquad (4)$$

Since the velocity is now complex, the same is true of the Lagrange function and therefore of the action. The generalization to a complex velocity $\mathcal{V}$ does not modify the form of the classical Euler-Lagrange equation ([21], [22]), but now, the classical differential operator d/dt is replaced by the complex differential operator d'/dt

$$\frac{d'}{dt}\frac{\partial L}{\partial \mathcal{V}_i} - \frac{\partial L}{\partial x_i} = 0. \qquad (5)$$

Let μ be the mass of the particle. In the case of a Newtonian closed system in a scalar field which is considered here, the Lagrange function becomes $L = \frac{1}{2}\mu\mathcal{V}^2 - \Phi$. This leads to a motion equation that conserves the form of Newton's fundamental equation of dynamics

$$\mu\frac{d'}{dt}\mathcal{V} = -\nabla\Phi, \qquad (6)$$

which is now written with complex time derivative operator and complex velocity. The complex velocity $\mathcal{V}$ still depends on the complex action according to the standard form ($\mu\mathcal{V} = \nabla\mathcal{S}$). Let us now make a change of variable, and define the function:

$$f = \exp\left(\frac{i\mathcal{S}}{2\mu\mathcal{D}}\right). \qquad (7)$$

In terms of this function, the fundamental equation of dynamics now writes

$$2i\mu\mathcal{D}\frac{d}{dt}(\nabla \ln f) = \nabla\Phi. \qquad (8)$$

By replacing in this equation the complex derivative operator by its expression (Eq. 3), one finds that it becomes

$$-2\mathcal{D}\nabla\left(i\frac{\partial}{\partial t}\ln f + \mathcal{D}\frac{\triangle f}{f}\right) = -\frac{\nabla\Phi}{\mu}. \qquad (9)$$

The real and the imaginary part of this equation can be separated. Indeed, the complex action is rewritten $\mathcal{S} = S + iS'$, and so, the function (f) takes another form:

$$f = \exp\left(\frac{i(S + iS')}{2\mu\mathcal{D}}\right) = \sqrt{\rho}\,\exp\left(\frac{iS}{2\mu\mathcal{D}}\right), \qquad (10)$$

with S the classical action which is connected to the classical velocity: $\mu V = \nabla S$. Finally, the real and imaginary part of the motion equation induce the following system of equations

$$\mu\left(\frac{\partial}{\partial t} + V \cdot \nabla\right)V = -\nabla(\phi + Q), \qquad (11)$$

$$\frac{\partial\rho}{\partial t} + \operatorname{div}(\rho V) = 0. \qquad (12)$$

The first one is a standard Euler-Newton equation but with the appearance of an additional potential energy term Q that writes:

$$Q = -2\mu\mathcal{D}^2\frac{\triangle\sqrt{\rho}}{\sqrt{\rho}}, \qquad (13)$$

and which is a manifestation of the fractal geometry. The second one is the continuity equation. We have therefore recovered the current minimal equations which are used in the standard hydrodynamical description, except for the new potential term. In the limit where the fractal fluctuations vanish, i.e. $\mathcal{D} \to 0$, the potential energy Q vanishes and the description is exactly reduced to the standard one. But conversely, the introduction of this new potential energy allows one to integrate the hydrodynamics equation under the

form of Eq. 9, which has the advantage to be linear and to allow the obtaining of analytical solutions.

The generalized hydrodynamical system obtained above can now be used as motion equation for a large class of systems [8], namely, all those coming under the three conditions that underlie its demonstration: large number of possible trajectories, fractal dimension 2 of trajectories, and local irreversibility. Actually these conditions amount to a loss of information about angles, position and time. But, paradoxically, such a total loss of information on the individual trajectories results in a tendency for self organization and structuration of the systems [22].

3 Theoretical development: spherical potentials

3.1 Symmetry constraints

The resolution of physical problems depends on the conservation laws imposed by the symmetries to which the physical system under consideration is subjected. As a first step, we shall consider spherically symmetric systems. Then, for a more complete study, other symmetries will be explored, in particular axial symmetrical systems. Moreover, the elementary approximation about the spherical potentials will be enriched by taking into account dynamical perturbations. These various effects are accounted for in a simple way by a specific choice of the coordinate systems (e.g. elliptic, parabolic or cylindrical).

Let us consider a test particle ejected by a star, submitted to various forces described by potentials (φ_i). Its motion is described by the hydrodynamical equation Eq.11:

$$\mu\left(\frac{\partial}{\partial t} + V \cdot \nabla\right)V = -\nabla\left(\sum\varphi_i + Q\right), \qquad (14)$$

Such a system is expected to be subjected to gravitational, radiative pressure, electromagnetic, and collisional forces.

However, in order to simplify the description we shall base ourselves on a fundamental observational result concerning these objects: the observations of the shells of many PNe's have shown that the expansion velocity is nearly constant. Such a result is already used in many numerical simulations ([7], [10], [15]). This means that, in the first order approximation (neglecting the interaction with the ISM), there is a dynamical compensation between the various forces acting on the shell, in particular between the gravitational force and the radiative stellar pressure. We shall therefore assume, as a first simplifying step, that the potential is

almost constant. We take the constant velocity approximation (i.e. free test particles) as a starting point for the following developments: In a second step, the model will include elements of perturbation such as velocity expansion to second order and the first order of perturbation power-series expansion (magnetics contributions and interactions with the ISM).

Therefore, we consider the generalized hydrodynamical equation with a vanishing potential:

$$\mu \left(\frac{\partial}{\partial t} + V \cdot \nabla \right) V = -\nabla(Q), \tag{15}$$

The velocity seems to be invariant during the ejection process. To simplify the search of stationary solutions, it is easier to rewrite the Euler-Newton/continuity system (Eq. 11, Eq. 12 depending on the variables $[\rho, V]$) in terms of a unique complex equation (depending on the variables $[\mathbf{r}, t]$) since it takes a Schrödinger-like form, for which several analytical solutions are known. This equation emerges from the integration of Eq.9 and writes ([20], [6])

$$\mathcal{D}^2 \triangle f + i\mathcal{D} \frac{\partial f}{\partial t} - \frac{\Phi}{2\mu} f = 0. \tag{16}$$

In a constant potential, stationary solutions of the form $f(\mathbf{r}, t) = g(\mathbf{r}) \, exp(-iEt/2\mu\mathcal{D})$, can be searched, and we obtain:

$$2\mu \mathcal{D}^2 \triangle g(\mathbf{r}) - E g(\mathbf{r}) = 0, \tag{17}$$

where $E = p^2/2\mu = 2\mu\mathcal{D}^2 k^2$ is the energy of this free particle. If we take a constant potential different from zero, we obtain the same equation but with a different particle momentum. The property of the Laplacian in the spherical coordinates governs the use of the spherical harmonics (which are common functions of L^2 and L_z). The general solution is now constrained by the conservation of the angular momentum and we can take a solution of the form $g(\mathbf{r}) = R(r) \, Y_l^m(\theta, \phi)$, where l and m are integers. The radial part is solution of the equation

$$R''(r) + \frac{2}{r} R'(r) + \left[k^2 - \frac{l(l+1)}{r^2} \right] R(r) = 0. \tag{18}$$

Two radial solutions of this free particle equation are known [17]:

$$R_{kl}^{\pm}(r) = (-1)^l A \frac{r^l}{k^l} \left(\frac{1}{r} \frac{d}{dr} \right)^l \frac{e^{\pm ikr}}{r}. \tag{19}$$

These functions can be developed in terms of the first order Hankel functions, namely

$$R_{kl}^{\pm}(r) = \pm i A \sqrt{\frac{k\pi}{2r}} H_{l+\frac{1}{2}}^{(1,2)}(kr), \tag{20}$$

which represent divergent spherical waves (+ case, with first order Hankel function) or convergent spherical waves (− case, with second order Hankel function). Divergent spherical waves can correspond to a flow of central particles emission and the convergent one to an infall flow of particles (we can already note that the physical solutions are totally reversible: this particular behavior will be developed in a forthcoming section). The normalization condition restricts the value of the constant, so that $A = 1/\sqrt{2\mathcal{D}k}$. The square of the modulus of the function f gives the probability density:

$$|g(\mathbf{r})|^2 = |R_{kl}(r)|^2 |Y_l^m(\theta, \phi)|^2. \tag{21}$$

We expect the true matter distribution to follow preferentially the peaks of this probability density distribution.

Now, this equation represents the distribution of potential trajectories for particles ejected during a unit time. But our aim is to know the evolution of these trajectories for distances and times higher than the ejection area. As a first step, the emitted particle flow can be considered to be only radial. Thus, the progression of the flow is free along the radial coordinate, and only the radial part of the function depends on the time variable. Thus the progression of the maximum probability can be approximately described as a spherical wave front with a constant velocity V_0. The time dependent function simply reads:

$$g(\mathbf{r}, t) = \frac{1}{r^2} R_{kl}(r - V_0 t) Y_l^m(\theta, \phi). \tag{22}$$

The $1/r^2$ coefficient accounts for the dilatation of the elementary shell.

3.2   Effect of perturbations

Let us now go on with our progressive method and include, for a more complete description, the perturbative potential terms.

First, one can relax the hypothesis of constant velocity by the consideration of a power series expansion of the radial velocity. These radial perturbative terms only affect the radial part of the spherical potential. Then this restriction will only change the radial part of the solution, but not the angular part. The information about the matter density distribution along the shells is related to the ejection history, while the global shape (which is observed in the end) is given by the angular distribution of matter (theoretically described in our framework by spherical harmonics). Thus, the principal actors of the structuration are the symmetries of the system. We can generalize this argument by including all kind of radial perturbative potentials (compatible with ejection processes) without any change in the result obtained about morphogenesis.

Other perturbations could affect the global process. We describe, hereafter, the effect of two of them:

• *Self gravitation:* The test-particle ejection associated with bipolar solutions (initially associated with bipolar axisymmetrical spherical harmonics) evolves through a new dynamical perturbation field linked to the axial symmetry. A self gravitational potential is created by the initial cylindrical repartition: each particle is subjected to a perturbative force in $-1/\rho^2$ (where ρ is the radial cylindrical coordinate). This attractive gravitational force constricts the ejection cone toward the symmetry axis of the system.

• *Magnetic field:* A magnetic contribution must be introduced in terms of a perturbative field. Strong magnetic fields are naturally associated with several stellar stages (e.g. red-giant stars and white dwarf stars [14]). A poloidal field can be introduced, as a first approximation, and the evolution of ionized particles (because of the UV radiation) is described by the same dynamics: a constriction along the axial system symmetry.

4 Results and comparisons to the observational data

4.1 Theoretical results

The main result obtained in the present work is the expected discretization of the possible shapes and the quantization of conservative quantities associated to the various predicted morphologies.

Let us first consider the main conservative quantity, i.e., energy. The energy to mass ratio ($E/m = 2\mathcal{D}^2 k^2$) is not quantized in this case, since there is no boundary condition to restrict the value of the particle wave vector (k). However, one will be led in future developments to consider the connection between the initial ejection process and the internal star structure. This work could provide a restriction of the wave vector possible values.

The second and the third prime integrals (consistent with the spherical coordinates) involve a quantization of the square of the reduced angular momentum and of its projection on the z axis, namely, $(L/m)^2 = 2l(l + 1)\mathcal{D}^2$ and $L_z/m = 2m\mathcal{D}$, which are independent of the test mass. The ratio $L/L_z = \sqrt{l(l + 1)}/m$ is also independent of the scale-parameter $\mathcal{D}$. Thus, this relation gives a general description of the angular momentum conservation law in all spherical ejection processes, independently of the specificity of the underlying fractal process.

The interpretation of these solutions is that the matter is expected to preferentially fill the high probability regions, as defined by the geometry of the geodesics (provided there is a sufficient quantity of ejected matter). Thus, one can directly associate a quantized structure with the angular functions. Moreover, as we shall now see, spherical harmonics involve also a quantization of other observables (i.e., the existence of peaks in their probability density distribution).

The θ angle is also subjected to a probability density distribution that have quantized peaks. This angle is observable in terms of the initial ejection angle (in the nearest central area, where the perturbations are insignificant). Concerning the remaining structure, the theoretically predicted value of the angle is no longer observable since the perturbation effects (studied above) result in a deformation of the shape toward the symmetry axis of the system. Another consequence of using spherical harmonics for the morphology description is the dependence of the matter density distribution on the angle quantization. For each component of the system (i.e. axial ejections, bipolar shells or equatorial discs), one can predict an initial ejection angle probability and a relative matter density distribution (relative to the other components of the matter distribution). All these results about the expected more probable values of the observable variables are summarized in Table 1: For each couple (l, m), we give the most probable values of the ratios L^2/m, L_z/m and we plot the associated angular solutions, $\rho(\theta) = |Y_l^m(\theta, cst)|^2$ (in a simplified form that takes account of the symmetry under the ϕ rotation).

Another important information in this table concerns the ratios of the amplitudes of the probability peaks for the ejection angles. The relative matter density between the imbricated conic structures (see Table 2) is expected to be proportional to the relative probability density: such a theoretical expectation can be put to the test (by an analysis of the luminosity ratios) in the observational data (see example hereafter).

The various shapes allowed by the generalized hydrodynamical solutions are presented in Table 2. The bipolar shells are plotted with a weak deviation toward the axis of symmetry. This deviation is typical of the various perturbative effects considered here-above (e.g., self gravitation, magnetic field).

4.2 Comparison with observational data

4.2.1 Planetary nebulae

As recalled above, the allowed shapes only depend on the (l, m) couple. Thus, the expected morphologies are no longer a consequence of the only initial conditions; they are mainly linked to the values of the conservative quantities and related to the angular boundary conditions. Similar basic hypotheses allow one

$\rho(\theta) = \lvert Y_l^m(\theta, cst)\rvert^2$	$m=0$ $L_z/m = 0$	$m=1$ $L_z/m = 2\,\mathcal{D}$	$m=2$ $L_z/m = 4\,\mathcal{D}$	$m=3$ $L_z/m = 6\,\mathcal{D}$	$m=4$ $L_z/m = 8\,\mathcal{D}$	$m=5$ $L_z/m = 10\,\mathcal{D}$	$m=6$ $L_z/m = 12\,\mathcal{D}$	$m=7$ $L_z/m = 14\,\mathcal{D}$
$l=0$ $(L/m)^2 = 0$	0, 90, 180							
$l=1$ $(L/m)^2 = 4\,\mathcal{D}^2$	0, 90, 180	45, 90, 135						
$l=2$ $(L/m)^2 = 6\,\mathcal{D}^2$	0, 90, 180	31, 90, 149	55, 90, 125					
$l=3$ $(L/m)^2 = 8\,\mathcal{D}^2$	0, 63, 117, 180	24, 69, 111, 156	41, 90, 139	60, 90, 120				
$l=4$ $(L/m)^2 = 10\,\mathcal{D}^2$	0, 49, 90, 131, 180	19, 56, 90, 124, 161	33, 72, 108, 147	47, 90, 133	63, 90, 117			
$l=5$ $(L/m)^2 = 12\,\mathcal{D}^2$	0, 40, 73, 107, 140, 180	16, 47, 76, 104, 132, 163	28, 60, 90, 120, 152	39, 74, 90, 106, 141	51, 90, 129	66, 90, 114		
$l=6$ $(L/m)^2 = 14\,\mathcal{D}^2$	0, 34, 62, 90, 118, 146, 180	14, 41, 66, 90, 114, 139, 166	24, 52, 77, 103, 128, 156	33, 63, 90, 117, 147	43, 76, 104, 137	54, 90, 106	68, 112	
$l=7$ $(L/m)^2 = 16\,\mathcal{D}^2$	0, 29, 54, 78, 90, 102, 126, 151, 180	14, 41, 66, 90, 114, 139, 166, 186	24, 52, 77, 103, 128, 156	33, 63, 90, 117, 147	43, 76, 104, 137	54, 90, 106	68, 112	90

Table 1: Synthesis of the quantized values of the squared angular momentum L^2/m, of its projection along z axis L_z/m, and of the matter distribution along quantized angles $\rho(\theta)$, associated with the angular wave functions Y_l^m, for the l and $m = 1$ to 7.

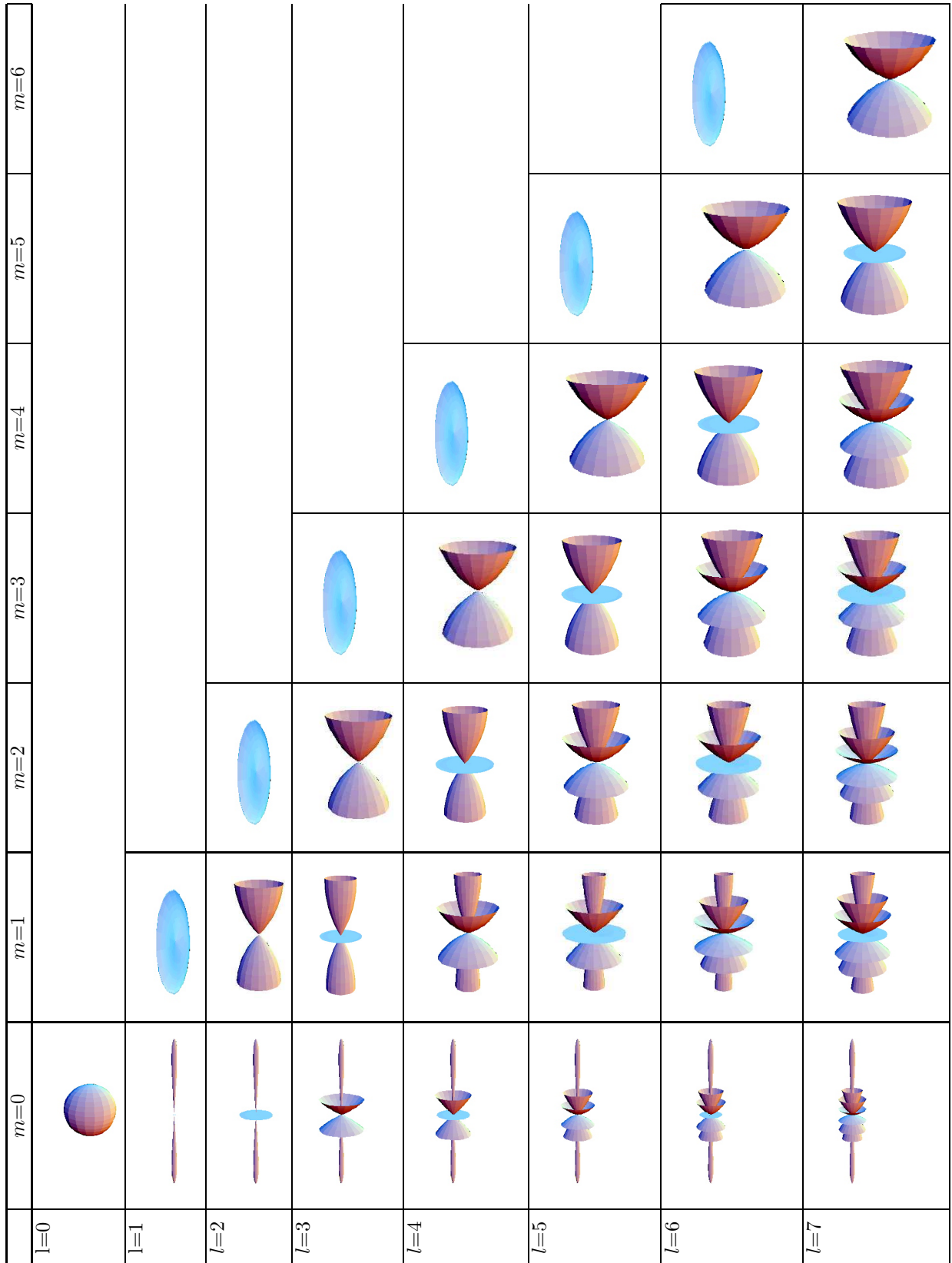|	m=0	m=1	m=2	m=3	m=4	m=5	m=6
l=0							
l=1							
l=2							
l=3							
l=4							
l=5							
l=6							
l=7							

Table 2: Synthetic representation of the first quantized shapes resulting from the angular ejections solutions given in (Table 1). Note the analogy of structure of the shapes along diagonals, i.e. $l - m = k$ =cst, which are characterized by the same number of imbricated cones, and differ only by the values of the angles. Note also that the theoretically predicted density significantly varies between the cones (see the corresponding figures in Table 1).
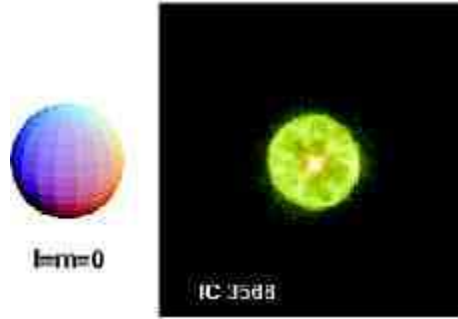
Figure 1: The elementary isotropic structure emerges from the fundamental level of the angular quantization law $(l = 0, m = 0)$. Left hand side: theoretical prediction. Right hand side: the spherical planetary nebula IC 3568.
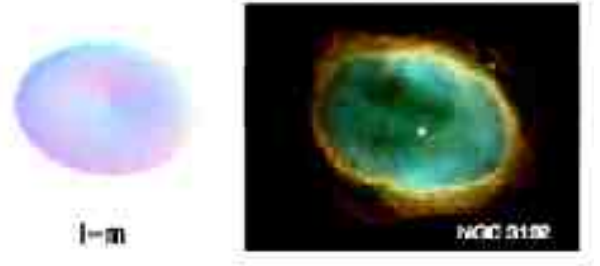

Figure 2: For some values of the inclination, the theoretical equatorial disc (left hand side) could appear like an elliptic PN. For example, NGC 3132 is observed elliptic, but there is still discussions about its true morphology (Monteiro et al. 2000).

to understand the constitution of bright shells in the spherical, elliptic and bipolar planetary nebulae. For remaining uncommon morphologies, various perturbations could be included in the active potentials. Moreover, more complicated symmetries (linked to other dynamical conservation laws) remain to be explored.

A new morphological description of planetary nebulae:

• *Spherical*: For a (l, m) couple equal to $(0, 0)$, one expects an isotropic matter distribution. This elementary case reflects the properties of the spherical planetary nebulae which were first discovered.

• *Elliptic*: All the solutions consistent with $(l = m)$ involve an equatorial disc structuration. With different tilting on the line of sight, elliptic shapes emerge from this solution. It is important to note that elliptic shapes can also result from perturbed spherical shapes, in accordance with the ISW model for elliptic shapes. Moreover, provided some apparently elliptic shapes are indeed the result of such a projection effect of disk structures, one expects to observe one day extremely flattened elliptical PNe: however, up to now this kind of PNe have not yet been observed (to our knowledge).

• *Bipolar*: Bipolar shapes emerge naturally from this work. These shapes are, in the standard approach, explained in terms of various effects such as different density outflows, presence of a double star system, etc... The present approach does not contradict these views: we simply connect the shapes directly to the state of the system, as described in terms of its conservative quantities (at first, the state of angular momentum). Whatever the particular cause for the system to jump to this state (which can be the presence of a second star, etc...), the same shape is expected to be observed for a given state. Moreover, this result generalizes the ISW model principles that lead to bipolar structures,
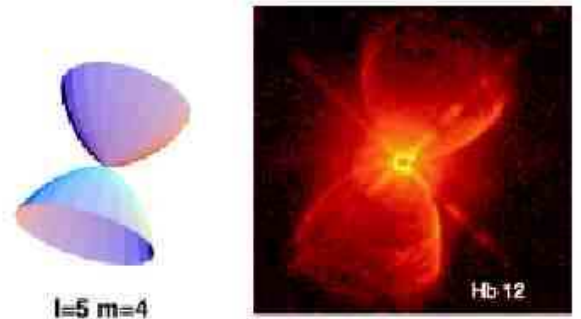
Figure 3: Elementary bipolar structure: the simple shell structure. The predicted $(5, 4)$ quantization with an initial angle of $63°$ is consistent with the observed structure of the planetary nebula $Hb12$.

since the free particles in bright shells could be directly issued from wind shocks (which are not conserved in standard models).

The first bipolar structure allowed by the possible values of the angular momentum is the simple shell one. This kind of simple situation can be illustrated by the planetary nebula $Hb12$ (fig. 3). The initial angle is consistent with a $(l = 5, m = 4)$ quantization (near $63°$) but this value is not sufficiently well measured to specify the quantum numbers with certainty (with regard to the nearest possibilities: $(l = 4, m = 3)$ or $(l = 6, m = 5)$).

Bipolar shapes become more complicated when the angular momentum increases. Beyond simple shells $(m = l - 1)$, bipolar shells with equatorial disks emerge in the same way $(m = l - 2$, cf the $Hb5$ structure).

The next case (fig. 4) is the double-shell planetary nebula of the M2-9 type. This shape is naturally expected from our classification, as corresponding to $m = l - 3$ (table 2). The morphology of M2-9 can be associated to the quantum numbers $(5, 2)$ (cf. ta-
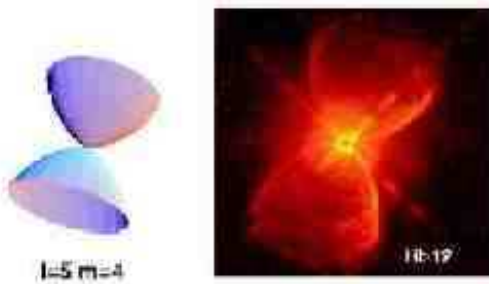
Figure 4: Double shell structure: the M2-9 planetary nebula can be associated with an angular momentum quantization of quantum numbers ($l = 5, m = 2$).
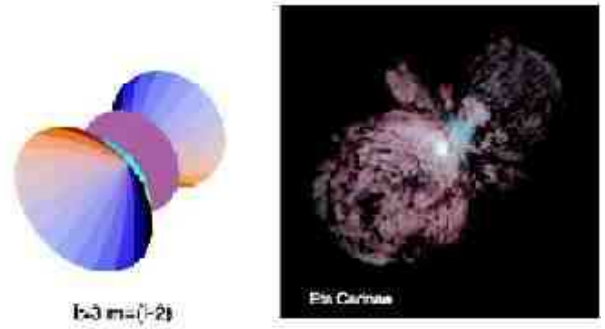

Figure 5: Generalization to another singular stellar systems: comparison between theoretical shapes with simple bipolar shell/equatorial disc and a LBV star (Eta Carinae).

ble 1) which involves a quantized angular distribution around the values ($33°, 72°, 108°, 147°$) and a higher density for the inner shells. The PN structure near the central star is not clearly defined, but the extrapolation of the external shell allows us to estimate the values of the initial ejection angles. This estimation ($\approx 30°$ for the outer shell and $\approx 70°$ for inner one) is consistent with the predicted angles: moreover, the inner observed density is clearly higher than the outer shell density, as theoretically expected.

Even more complex (therefore less probable) structures that have not been observed up to now, are still possible: double-shell + disk ($m = l - 4$), triple-shell ($m = l - 5$), etc... In all these new cases, as for the already observed ones, the theoretical prediction applies not only to the overall morphology, but also to quantitative values of angles, angular momenta and density distributions, and it will therefore be possible to put it to the test in the near future.

4.2.2   LBV stars

The theoretical development presented in the first part of this paper is associated with a general ejection process. Luminous blue variable (LBV) stars are in essence very different from PN central stars. Despite of this internal incompatibility, some recent works [11] have been developed to explain the shell formation around LBV stars by the same hydrodynamical ISW model that was used for planetary nebulae.

Therefore the method studied in the present paper can be applied to a morphological description of these objects. In consequence we also expect a quantization of quantities such as angular momenta and angles and a discretization of the possible shapes for the matter density distribution around LBV stars. For example, the Eta Carinae LBV star shows bipolar shell with an equatorial disk (fig. 5: such a structure is expected in all the cases when $l > 3$ and $m = (l - 2)$). Therefore this result supports the idea of a general behavior

of ejection processes and of the self-similarity of shell structurations, independently of the nature of the central star.

4.2.3   Supernovae

There are other systems that can be analyzed with this new point of view, in particular supernova remnants. Whatever the specific ejection process at work in supernovae (Ia or II..), the three conditions upon which our method relies, namely (i) fractal trajectories, (ii) infinity of potential trajectories, (iii) time-reflection breaking, are expected to be achieved in this case, since the same collisional/diffusing processes as for planetary nebulae are present. Moreover, the here-above theoretical developments can be generalized to scattering systems described by an initial convergent wave function (as in implosion processes) and by a resultant divergent wave function (ejection processes). Supernova structures emerge from the interaction of remnant matter from the central star explosion and the ISM. This simple presentation suggests a behavior of SNe particles which may be similar to ejected particles in PNe or LBV stars. Thus, provided the ISM interaction is assumed to be homogenous (as a first order approximation), the quantized results obtained by the theoretical development (table 2) are still valid. The account of inhomogeneities of the ISM would be more difficult, since they degrade the initial conserved information on prime integrals and then, would involve a more complicated description. One of the most enigmatic SN is SN-1987A (Fig. 6). Its particular structure (which has up to now resisted to all hydrodynamical simulations) can be accounted for by a unique ejection associated with a quantized angular momentum corresponding to $m = l - 2$ (see Table 2). This configuration induces, in the case of a discontinuous ejection process,
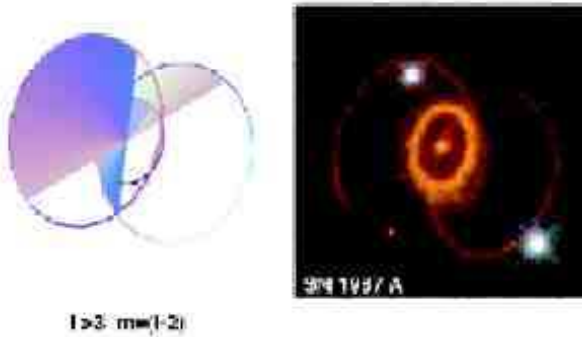
Figure 6: Simple model of supernova remnant: as a first order approximation, one finds that supernovae remnants could also be structured like other spherical ejection systems. For a single ejection phase, this leads to the formation of expanding rings, that are expected to be ejected with higher probability along given angles.

Figure 7: An example of morphology observed in a star formation process, compared with a theoretically predicted possible structure.

a geodesic structuration into two bipolar rings and an equatorial ring, as observed. Moreover, in recent images the central star is projected on the right ring. In such a configuration, the ejection cone angle is given by $\cos(\theta) = b/a$ where a and b are respectively the major and minor axes of the projected ellipse. From 6 measurements on the inner edge, middle and outer edge of the equatorial ring and of the right polar ring (the left ring was not used because it shows distortions to ellipticity), we find $\theta = 41.2 \pm 1.0$ deg, which supports the identification with the case $m = 2, l = 4$, for which the predicted angle is 40.89 deg (while the nearest similar configurations yield 31 deg and 47 deg). The youth of the system (10 years compared with 10^4 years for typical PNe) supports the assumption that the observed angle is still the initial ejection angle.

From this preliminary work, we suggest that future observations of young supernovae in homogeneous ISM will allow one to put the theory to the test in a quantitative way, since we expect the occurrence of quantized structures consistent with the general results given in Table 2.

4.2.4   Star formation

Low mass star formation processes seem to be universally associated with circumstellar infall / accretion discs and outflow / axial ejections ([1], [5]). In the standard approach, the existence of such simultaneous structures is still not fully understood (despite several attempts using various magnetic models [12]).

The solutions associated with free motion in spherical potentials describes either convergent or divergent
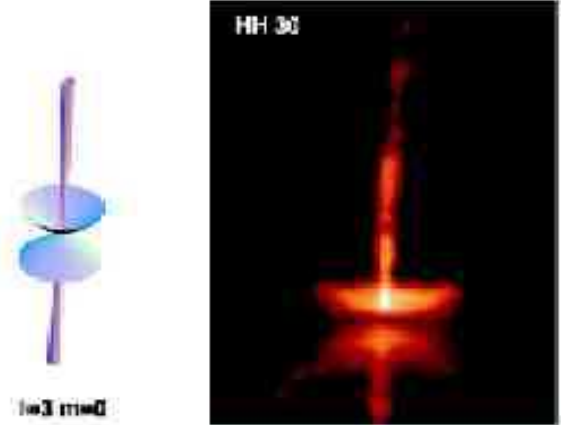
spherical waves (eq. 19). From the point of view of the present theoretical description in terms of probability amplitudes, the two cases of ejection and accretion both correspond to a scattering process (one simply reverses the sign of time). It is therefore quite simple to consider solutions that combine accretion (for example, equatorial) and ejection (fro example, polar).

One cannot make any longer the hypothesis of free motion in an accretion phase. However, this concerns only the radial dependence of the solutions, while the angular dependence is still expected to be given by spherical harmonics. Finally, in a typical star birth stage, the above method is able to account for the observed discretized structuration of the infall matter and of the resultant particle ejection.

For example the HH-30 observations (Fig. 7) allow us to make a preliminary analysis of this proposal. The equatorial disc and the resultant axial ejection agree with the morphology given by $l = 1$, $m = 0$ for axial ejection and $m = l$ for the accretion disc. The global angular momentum is conserved during the scattering process, but the L_z behavior is still an open problem (since it could be described by a more complex solution like $(l = 2, m = 0)$). The bright bipolar shells are currently considered as reflection nebulae [4], but this component could also have a different dynamical behavior (with respect to the equatorial disc) and thus could correspond to a solution like $(3, 0)$ or $(4, 0)$. We present in Fig. (7) the structure closest to observations allowed by the theoretical developments.

5   Conclusion and prospect

In this paper, we have given a general description of matter structuration in spherically symmetric poten-

tials. The motion equation, rewritten in terms of an hydrodynamical system which incorporates the equation of continuity, depends directly on the conditions of symmetry of the system.

In the case of spherical symmetry, which is the situation mainly considered in this study, the solutions depend on the values of the conservative quantities (E, L^2 and L_z). This method leads to a great diversity of stationary solutions, that are expected to describe infall and ejection motion from central bodies, in terms of probability density distributions for the radial distance and the values of the ejection (or accretion) angles.

In the case when the potential depends only on the radial coordinate, the general solutions (which give the density of potential trajectories) are then separable in a radial $R(r)$ and a spherical part given by the spherical harmonics $Y_l^m(\theta, \phi)$. The possible morphologies are therefore classified according to the values of the integer numbers l and m. Thus, most probable quantized structures (table 2) result from the angular probability distributions (table 1) and can be compared with the various systems that come under such a description (planetary nebulae, LBV stars, supernovae, young star formation). Moreover, the theoretical approach allows one to predict the possible existence of structures that have no yet been observed, and of yet unidentified correlations between the morphology and observable quantities.

Let us conclude by some examples of possible future extensions of the present study:

- The connection between internal stellar structures and the ejection process could provide informations about the probability distribution of the velocity ejection.

- Concerning the planetary nebula description, the internal stellar angular momentum is known to be structured: various external quantized solutions are then possible. The internal structuration could induce an external combination of spherical harmonic solutions (depending on the ejection history).

- Particular quantized solutions (l, m) can be connected with the central system and show a dependence on specific conditions (single star with inclined magnetic fields, double star system etc..).

- Several simple systems present axial symmetry: therefore several new possibilities of morphogenesis can be explored by considering other coordinate systems (e.g. cylindrical symmetry, parabolic symmetry etc..).

- Only hints about the perturbation effects have been given here: future work is needed in order to introduce the perturbation potential in the Euler-Newton / continuity equation (non trivial solutions).

- Numerical simulations using the above solutions as initial conditions can be performed, in order to study the influence of perturbation fields (e.g. magnetic contribution, self-gravitation, ISM interaction...), and to explore the possibility of appearance of nontrivial structures.

Acknowledgments

References

[1] André Ph., 2002, Star formation and the physics of young star, Bouvier J., Zahn J.P. (eds.), EAS Publications Series, 2, 1

[2] Balick B., 1987, AJ, 94, 671

[3] Balick B., 2000, Asymmetrical Planetary Nebulae II, ASP Conference Series, 199, 41

[4] Burrows, C.J. et al., 1996, ApJ, 473, 437

[5] Cabrit S., 2002, Star formation and the physics of young star, Bouvier J., Zahn J.P. (eds.), EAS Publications Series, 2, 147

[6] Célérier M.N., Nottale L., 2003, Electromagnetic Phenomena T. 3, N1 (9), 83. eprint hep-th/0210027.

[7] Corradi R.L.M, 1999, A&A, 354, 1071

[8] Da Rocha D., Nottale L., 2003, Chaos Solitons & Fractals, 16, 565

[9] Dyson J., de Vries J., 1972, A&A, 20, 233

[10] Dwarkadas V., Chevalier R., 1996, ApJ, 457, 773

[11] Dwarkadas V., Balick B., 1998, AJ, 116, 829

[12] Ferreira J., 2002, Star formation and the physics of young star, Bouvier J., Zahn J.P. (eds.), EAS Publications Series, 2, 229

[13] Franco J., Garcia-Segura G., Lopez J.A., Kurtz S., 2002, RevMexAA, 12, 127

[14] Garcia-Segura G. et al., 1999, ApJ, 517, 767

[15] Garcia-Segura G., Lopez J.A., Franco J. , 2001, ApJ, 560, 928

[16] Kwok S., Purton C.R., Fitzgerald P.M., 1978, ApJ, 219, L125

[17] Landau L., Lifchitz E., 1967, Quantum Mechanics (Mir, Moscow)

[18] Mellema G., Frank A., 1994, ApJ, 430, 800

[19] Monteiro H., Morisset C., Gruenwald R., Viegas S.M.,2000, ApJ, 537, 853

[20] Nottale L., 1993, Fractal Space-Time and Microphysics: Toward a Theory of Scale Relativity. London: World Scientific.

[21] Nottale L., 1996, Chaos Solitons & Fractals, 7, 6, 877-938

[22] Nottale L., 1997, A&A, 327, 867